Aqueous Redox Flow Battery Suitable for High Temperature Applications Based on a Tailor-Made Ferrocene Copolymer

Philipp S. Borchers, Maria Strumpf, Christian Friebe, Ivo Nischang, Martin D. Hager, Johannes Elbert, and Ulrich S. Schubert*

Water-soluble, and ferrocene-containing methacrylamide copolymers with different comonomer ratios of the solubility-promoting comonomer [2-(methacryloyloxy)-ethyl]-trimethylammonium chloride (METAC) are synthesized in order to obtain a novel, temperature-stable electrolyte for aqueous redox flow batteries. The electrochemical properties of one chosen polymer are studied in detail by cyclic voltammetry and rotating disc electrode (RDE) investigations. Additionally, the diffusion coefficient and the charge transfer rate are obtained from these measurements. The diffusion coefficient from RDE is compared to the value from synthetic boundary experiments at battery concentrations, using an analytical ultracentrifuge, yielding diffusion coefficients of a similar order of magnitude. The polymer is further tested in a redox flow battery setup. While performing charge and discharge experiments against the well-established *bis*-(trimethylammoniumpropyl)-viologen, the polymer reveals high columbic efficiencies of >99.8% and desirable apparent capacity retention, both at room temperature as well as at 60 °C. Further experiments are conducted to verify the stability of the active compounds under these conditions in both charge states. Lastly, the electrochemical behavior is linked to the characteristics of the polymers concerning absolute values of the molar mass and diffusion coefficients.

P. S. Borchers, M. Strumpf, Dr. C. Friebe, Dr. I. Nischang,
Dr. M. D. Hager, Dr. J. Elbert,[+] Prof. U. S. Schubert
Laboratory of Organic and Macromolecular Chemistry (IOMC)
Friedrich Schiller University Jena
Humboldtstr. 10, Jena 07743, Germany
E-mail: ulrich.schubert@uni-jena.de
P. S. Borchers, M. Strumpf, Dr. C. Friebe, Dr. M. D. Hager, Dr. J. Elbert,
Prof. U. S. Schubert
Center for Energy and Environmental Chemistry Jena (CEEC Jena)
Friedrich Schiller University Jena
Philosophenweg 7a, Jena 07743, Germany
Dr. I. Nischang, Dr. M. D. Hager, Prof. U. S. Schubert
Jena Center for Soft Matter (JCSM)
Friedrich Schiller University Jena
Philosophenweg 7, Jena 07743, Germany

[+]Present address: Department of Chemical and Biomolecular Engineering, University of Illinois at Urbana-Champaign, Urbana, IL 61801, USA

1. Introduction

With renewable energies on the rise, the demand for cheap and reliable energy storage solutions is constantly increasing. Since photovoltaic or wind energy do not provide a steady energy output and because overproduction of electrical energy jeopardizes the stability of the electrical grid, the large-scale implementation of those technologies is challenging, making technologies for storing and releasing electrical energy on demand a crucial part of the electrical grid of the future worldwide.[1] Therefore, different challenges have to be overcome, e.g., long-term durability of the battery components and their stability during battery operation, which is in particular demanding in areas with elevated temperature conditions.

A promising solution for stationary energy storage systems are redox flow batteries (RFBs). RFBs have the advantage of the independent scaling of energy and power, thus allowing the use in private households, industrial plants, or even in large-scale grid-storage applications like wind parks.[2] The currently best developed redox flow systems for charge storage are based on vanadium ions as active compounds.[3] However, these systems require highly corrosive electrolytes and the utilized vanadium has a large CO_2 footprint and is considered a pollutant of emerging concern.[4] Additionally, vanadium-electrolyte-based systems require extensive cooling efforts to keep the temperature of the battery in a safe limit during standard operation, making them very energy-inefficient and leading to additional acquisition and maintenance cost.[5] As a consequence, efforts are made to establish less precarious active materials, such as zinc,[6] metal halides,[7] iron,[8] or the great variety of organic compounds,[9] which can be considered as more environmentally friendly and less toxic materials.
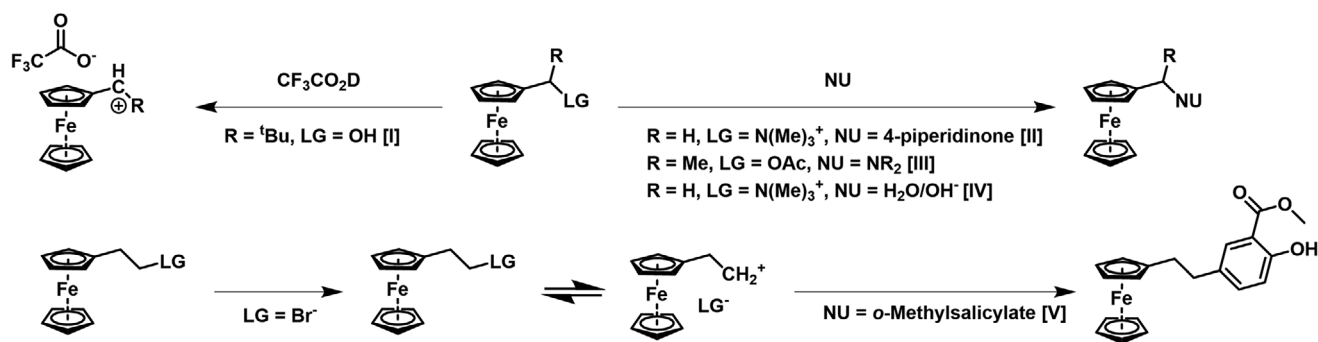
However, temperature-stability investigations of organic RFBs are scarcely conducted (see Chen et al.[10] for an exception) and, to the best of our knowledge, aqueous polymeric systems have never been examined under this point of view. Here we report on a greener, acid-free, high temperature RFB system suitable for potential applications in Africa, India, and other regions with elevated temperatures.

A very promising active material for battery applications is ferrocene. The iconic organometallic molecule is known for a long time for its remarkable redox stability and is, hence,

Scheme 1. Schematic representation of the instability of α and β substituted ferrocene derivates. LG = leaving group, NU = nucleophile, see I,[22] II,[23] III,[24] IV,[25] and V.[26]

commonly used as an internal standard for electrochemical measurements.[11] Since ferrocene contains the metal iron, it can still be considered less problematic in terms of market value, availability,[12] noted toxicity,[13] and pollution, when compared to other metals used in battery systems, such as vanadium, cobalt, and lithium.

Ferrocene can easily be functionalized by various established reactions, thus making it a very versatile materials platform. Due to its low toxicity, the attention of medical chemists was also drawn to ferrocene,[14] even leading to the development of promising drugs.[15] Ferrocene has also been thoroughly investigated in glucose sensing applications, where it works as an electron mediator between the organic system and a measuring electrode in typical aqueous environments.[16] Lately, ferrocene has been discussed for many energy storage applications, including solid-state batteries,[17] solid-state-flow hybrid batteries,[18] non-aqueous RFBs,[19] or all aqueous RFBs.[20] Additionally, liquid derivates have been considered as catholytes for flow batteries.[21] However, substituted ferrocene derivates are known to easily undergo substitution and elimination reactions in α and β position[22–26] (**Scheme 1**) in a nucleophilic environment like water. As a consequence, most of the recently reported ferrocene derivates are potentially unstable at higher temperatures or need cost intense cooling efforts, lowering the efficiency of the battery systems.

Polymers represent an interesting component for battery applications,[27] where they have been studied intensively as active materials in polymer RFBs.[28] Since polymers can be retained by a size-exclusion membrane, it is possible to replace the cost-intensive ion-selective membranes in RFBs.[29] Such membranes make up a substantial part of the overall costs,[28c] therefore using size-exclusion membranes could significantly lower the costs of the electric stack.[30] As an example, hydrophobic polymers were recently used to form electroactive particles in solution, which were separated with a size exclusion membrane, which showed excellent cycling behavior in battery applications.[31]

The incorporation of ferrocene in polymeric structures is known for a long time.[32] Recently, these polymers have been studied in supercapacitors,[33] solid-state batteries,[34] and organic RFBs.[30] Another well explored active material in polymeric materials for aqueous RFBs is the 2,2,6,6-tetramethylpiperidinoxyl (TEMPO) radical,[35] which shows acceptable performance in battery applications.

To the best of our knowledge, no temperature-stable, polymeric system incorporating ferrocene monomeric units has yet

been designed to be employed in aqueous RFBs. Particularly, after Aziz et al. have published an excellent battery system, which uses a small ferrocene molecule as an active material component,[20a] it appeared interesting to evaluate the performance of a ferrocene-containing polymeric architecture in an aqueous solution and to explore the stability of both the charged and the uncharged state of the electrolytes, with special focus on the thermal stability in those states and during cycling of the battery.

The main challenge in utilizing ferrocenes in aqueous RFBs is the extreme hydrophobicity of ferrocene in the uncharged state as well as the aforementioned stability issues of substituents in α and β position. Therefore, we synthesized a ferrocene containing monomer, which utilizes a C3 spacer between the ferrocene and a possible leaving group, thus preventing elimination or substitution reactions with water as solvent (**Figure 1**). By using an amide group as linker between the polymerizable group and the electroactive group, we enabled hydrogen bonds between the monomer and the solvent, thus enhancing its solubility. To further promote the water solubility, we copolymerized the ferrocene monomer with [2-(methacryloyloxy)-ethyl]-trimethylammonium chloride (METAC). Polymers with different ratios of the solubility mediator were synthesized and their solubility in water was evaluated to identify the optimal amount of solubility promoter. Electrochemical characterization using cyclic voltammetry (CV) and rotating disc electrode voltammetry (RDE) was conducted. The diffusion coefficient of
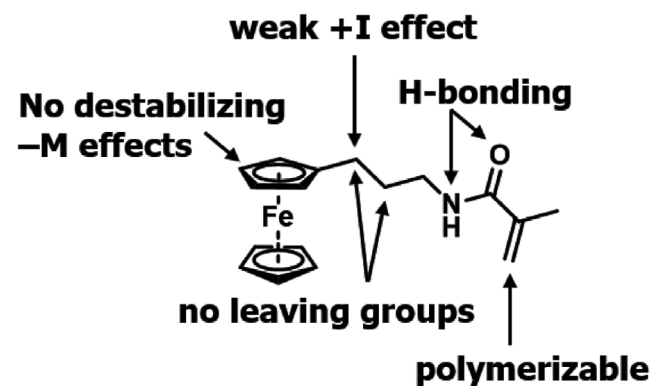
Figure 1. Design principle of the ferrocene monomer. I effect = inductive effect, M effect = mesomeric effect, H-bonding = hydrogen bonding.

a selected polymer was determined in an aqueous environment by RDE measurements as well as via complementary synthetic boundary experiments making use of an analytical ultracentrifuge as an orthogonal method. Finally, the performance of the new polymeric as a catholyte in an RFB was evaluated by battery charge-discharge cycling against the well-established[20a] 1,1-*bis*-[3-(trimethylammonium)-propyl]-4,4-bipyridinium tetrachloride (BTMAPV) as the anolyte at both ambient temperature and 60 °C. As temperature stability is crucial for RFB operation, special attention was paid to the durability of the charged as well as the uncharged electrolytes, which were analyzed with NMR experiments. We could prove that the chosen redox couple is not just stable, but its performance is even enhanced at elevated temperatures.

## 2. Results and Discussion

2.1. Polymer Synthesis

To overcome the challenge of dissolving the hydrophobic ferrocene in water, we aimed at copolymers with water-soluble comonomers. However, most of the well-known ferrocene monomers, such as vinyl ferrocene, copolymerize poorly with potential comonomer candidates. As a consequence, we targeted a ferrocene monomer which becomes well solvated with water via hydrogen bonding, thus promoting the desired water solubility, while being stable against high temperatures and nucleophiles at the same time. An obvious solution would be the esterification of hydroxymethylferrocene. However, such esters are reported to be unstable in aqueous solution,[36] which makes them unsuitable for the intended application. Furthermore, as ferrocene is known to stabilize cations in benzylic positions exceptionally well,[14] it is prone to elimination and substitution reactions in α and β positions, in particular at elevated temperatures. Therefore, we aimed at substitution at the γ position (Figure 1), which was enabled by the use of a propyl linker. Using an aliphatic linker ensured no interference of the linker with the ferrocene's π system via inductive effects (±I effects) or mesomeric effects (± M effects), thus not endangering the stability as well as the electrochemical properties of the redox-active material.

The synthesis of ferrocenylpropyl methacrylamide (FPMAm, 5) (Scheme 2) was based on early works by Khand et al.,[37] who synthesized the corresponding amine but carried out with carefully developed modifications in the synthetic procedure. Ferrocene carboxaldehyde (1), as an easily accessible[38] and commercial starting material, was condensed with acetonitrile in a nitrile aldol reaction to yield ferrocene acryloylnitrile (2). This species was selectively reduced to the corresponding amine via a two-step process. The first step was the reduction of the double bond with hydrogen and palladium, which yielded exclusively the 2-ferrocene-propionitrile (3). The nitrile was subsequently reduced with lithium aluminum hydride to yield the respective amine (4). The last step was the amide synthesis with methacryloylchloride, yielding the methacrylamide (5). An overall yield of 51% for the four-step sequence of reactions was obtained after optimizing all reaction steps. This reaction sequence was chosen as it provides access to the product from a commercially available starting material in a minimum number of steps. Furthermore, it avoids the use of problematic substances, which have been reported in the synthesis of the respective amine.[39] The synthesis route allows easy upscaling as it features a high overall yield, involves no complex reaction steps and the amine can be distilled.

For the intended use of the polymer in an aqueous RFB and due to the well-recognized hydrophobic nature of ferrocene, a very hydrophilic comonomer appeared necessary to provide sufficient water solubility at a neutral pH value. Therefore, the commercial METAC was used as a hydrophilic comonomer in a free-radical polymerization reaction. Different monomer stoichiometries (**Table 1**) were investigated to identify an optimal balance of ferrocene and comonomer regarding energy density (content of active material) and solubility (content of comonomer). Free-radical polymerization was chosen as the most straightforward polymerization technique, as it is suitable for methacrylamides, very robust, and cost effective. The polymerization reaction conditions (**Scheme 3**) were kept constant to enable a comparability of the different polymers obtained from the polymerization reactions (Figures S12–S16, Supporting Information).

Samples were taken at different times during the polymerization and the reaction was monitored by ^{1}H NMR. By plotting the double bond proton integral of the corresponding hydrophilic monomer versus the ferrocene signal integral (Figure S18, Supporting Information), the half-life for the METAC monomer 6 was found to be about 20 min, while the half-life for the FPMAm monomer 5 was ≈43 min under such conditions. These results revealed that FPMAm 5 is incorporated in the formed polymer approximately half as fast as the METAC 6 is, leading to a drift in the polymer composition. The polymerization reached an overall conversion of ≈90% of FPMAm 5 and a nearly full conversion of METAC 6 after 4 h. Overall, four different polymers with varying monomer ratios in the feed were synthesized under the exactly same reaction conditions.
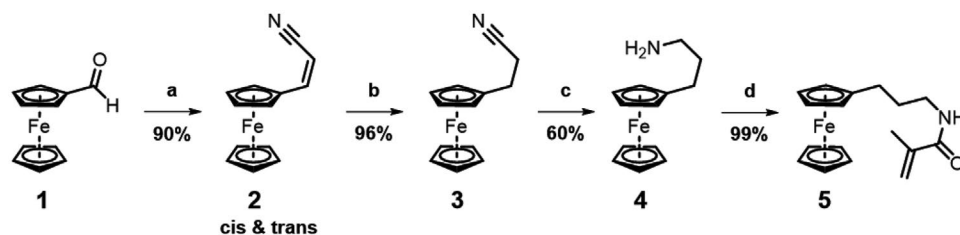
Scheme 2. Schematic representation of the synthesis of the FPMAm monomer 5. a) Acetonitrile/water, KOH, reflux, 4 h, b) Pd/C 10%, H$_2$ at 5 bar, EtOAc, 40 °C, 33 h, c) LiAlH$_4$, diethyl ether, 0 °C to 25 °C, 24 h, d) methacryloylchloride, NEt$_3$, CH$_2$Cl$_2$, 4 h.

**ADVANCED
SCIENCE NEWS**
www.advancedsciencenews.com

**ADVANCED
ENERGY
MATERIALS**
www.advenergymat.de

Table 1. Reaction conditions for the polymerizations, the resultant polymers, and some of their properties. ACVA = 4,4′-Azo-*bis*-(4-cyanovaleric acid).

	Monomer ratio [mol% FPMAm]		M_n [g mol^{-1}] (Đ)[c]	Solubility[d] [mol L^{-1}]
	Target[a]	Found[b]		
P1	20	13.5	11720 (1.93)	n.d.
P2	20	12.0	10940 (2.31)	>1.0
P3	50	32.5	7570 (1.33)	>1.0
P4	40	25	7990 (1.48)	>1.0
P5	30	19	6900 (1.50)	>1.0

For all experiments, the temperature was 80 °C, the time was 4 h and the initiator-concentration was 5 mol% with respect to the sum of monomers. [a]Targeted monomer ratio at the start of the reaction; [b]The ferrocene content was determined by cerimetric titration; [c]Determined by SEC in H_2O with 0.1 M NaCl + 0.1% trifluoroacetic acid and a poly-(2-vinylpyridine) calibration; [d]Values are given in mol of active ferrocene moieties per L of water.

Since quantification of the ferrocene content of the copolymers by ^1H NMR was difficult, the ferrocene content was determined by cerimetric titration (see Supporting Information for details). The solubility of all polymers was sufficient to realize solutions with >1 M ferrocene. Rather than the polymer solubility in water, the viscosity appeared to be the limiting parameter. It could be observed that 1 M active ferrocene moiety concentration of polymers in water resulted in gel-like consistency, while 0.5 M solutions appeared to be rather honey-like liquids.

The absolute molar mass of P2 was also determined via SEC-MALLS (Figure S28, Supporting Information) as described previously.[40] The weight-average molar mass was found to be 52 000 g mol^{-1} at an apparent dispersity of Đ = 2.

2.2. Electrochemical Characterization and Determination of the Diffusion Coefficient

P2 was used for a first electrochemical characterization. As an initial test, CV (Figure S19, Supporting Information) of the polymer was measured to determine the redox potential in an aqueous environment. The oxidation was found to take place at 570 mV and the re-reduction at 470 mV utilizing a scan rate of 50 mV s^{-1}, which results in a half-wave potential of $E_{1/2} = 520$ mV. This value is 130 mV above the value that Aziz et al.

published for a double-substituted small ferrocene molecule in water,[20a] which may be caused by the absence of an +I effect of one alkyl group into the cyclopentadienyl-ligand. The polymer revealed excellent cycling stability with a quasi-reversibile redox process for over 120 cycles and for six different scan rates (Figure S19, Supporting Information). The rather large difference in the electrochemical potential of the redox process may originate from changes in the polymer due to repulsive interactions in the charged polymer. BTMAPV 7 was added to the solution, to evaluate the potentials of the redox reactions present in the battery (**Figure 2**). BTMAPV was chosen as it has proven to be a very stable anolyte in RFBs.[20a]

The diffusion coefficient of the polymer in aqueous solution, the electron transfer rate, and the electron transfer coefficient were obtained by RDE measurements (Figure S20, Supporting Information).[28c] Analysis using the Levich equation resulted in an apparent diffusion coefficient of $D_{app} = 9.8 \times 10^{-7}$ cm^2 s^{-1} for polymer P2. Further analysis via the Koutecký-Levich plot and the Tafel plot yielded an electron transfer rate constant of $k^0 = 4.4 \times 10^{-6}$ m s^{-1} and an electron transfer coefficient of $\alpha = 0.60$.

In addition, the diffusion coefficient of polymer P2 was determined by synthetic boundary experiments making use of an analytical ultracentrifuge as described recently.[41] Therefore, we utilized the very same concentration of the polymer as used in the battery application. A measurement in pure water yielded an apparent diffusion coefficient of $D_{app} = 60.7 \times 10^{-7}$ cm^2 s^{-1} (Figure S29, Supporting Information). Repeated measurements confirmed this value, which is in a typical range of small molecules. This may be related to polyelectrolyte diffusion against pure water and, consequently, the contribution of a potential gradient to diffusion boundary dispersion. To mediate for the polyelectrolyte effect, the measurement was repeated in 0.1 M aqueous sodium chloride solution, which yielded a repeatable value of the diffusion coefficient value of $D_{app} = 7.6 \times 10^{-7}$ cm^2 s^{-1}. This value is in reasonable agreement to the diffusion coefficient which was identified by RDE investigations (vide supra) and is close to recent reports of diffusion coefficient values for a polymer of similar molar masses, e.g., a viologen-polymer ($M_n = 30.9$ kDa, Đ = 2.4) and a TEMPO-polymer ($M_n = 20.2$ kDa, Đ = 1.7), reported by Janoschka et al.[28c] The electron transfer rates of said polymers (4.5×10^{-6} m s^{-1} and 9×10^{-7} m s^{-1}, respectively) are close to the herein presented polymer with a value of 4.4×10^{-6} m s^{-1}. The electron transfer coefficient of $\alpha = 0.60$ can be considered fairly close to the ideal[42] value of $\alpha = 0.5$.
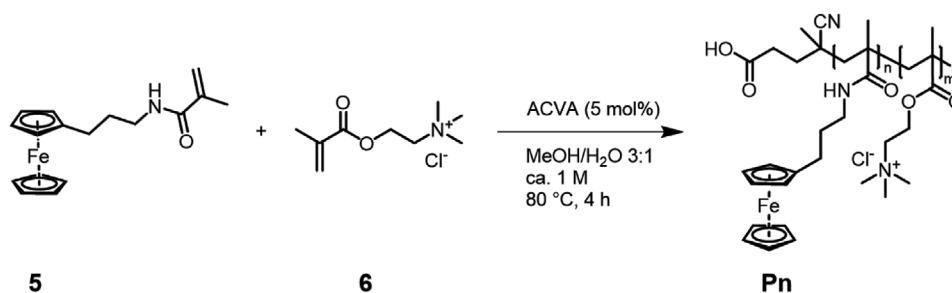
Scheme 3. Schematic representation of the free-radical copolymerization of FPMAm 5 with METAC 6 to yield water soluble, ferrocene-containing polymers. ACVA = 4,4′-Azo-*bis*-(4-cyanovaleric acid).
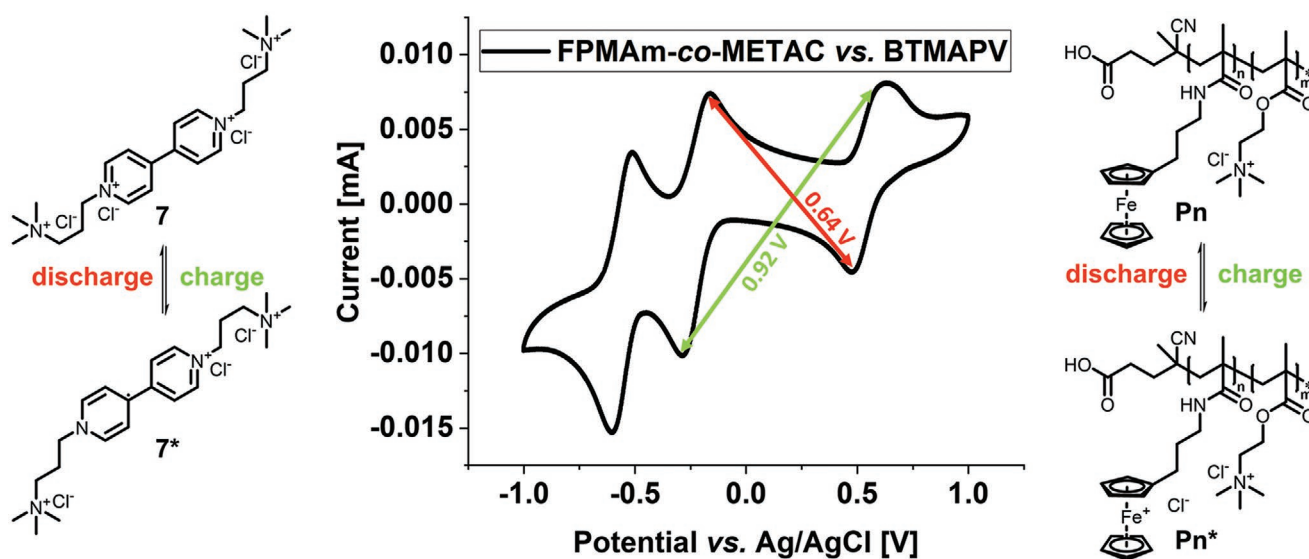
Figure 2. Schematic representation of the redox processes of the active materials and their behavior in cyclic voltammetry measurements in 0.1 M NaCl$_{aq}$ solution. A three-electrode setup was used with a glassy carbon working electrode, a platinum wire as the counter electrode, and a Ag/AgCl reference electrode. 200 mV s^{-1} scan rate from 0 to +1 V to − 1 V. The charging process is represented in green as the peak to peak potential in the voltammogram and the discharging process is depicted in red, respectively.

2.3. Battery Testing

Battery experiments were performed with P1 and BTMAPV 7 in an argon-filled glovebox. An excess amount (1.5 eq) of viologen 7 was used to prevent the possibility of an irreversible two-electron reduction of the bipyridyl moiety. The large amount of chloride in these molecules already provided sufficient conductivity of the solution for further testing. The electrolyte reservoirs were placed in a heatable sand bath to enable testing at elevated temperatures. A custom-made cell-stack[43] was utilized for the experiments, which comprises graphite felts that increase the available surface area of the graphite electrode, while filling the space to the membrane, and thus decreasing the effective distance from electrode to electrode for the current to pass. A FUMASEP FAA-3-50 anion exchange-membrane with an area of 5 cm² was used as the separator. Battery testing was initiated by measuring the setups resistance via potentiostatic electrochemical impedance spectroscopy (Figure S24, Supporting Information). The specific resistance was found to be ≈2 Ω cm², which is comparable with a battery operating with a small ferrocene molecule.[20a]
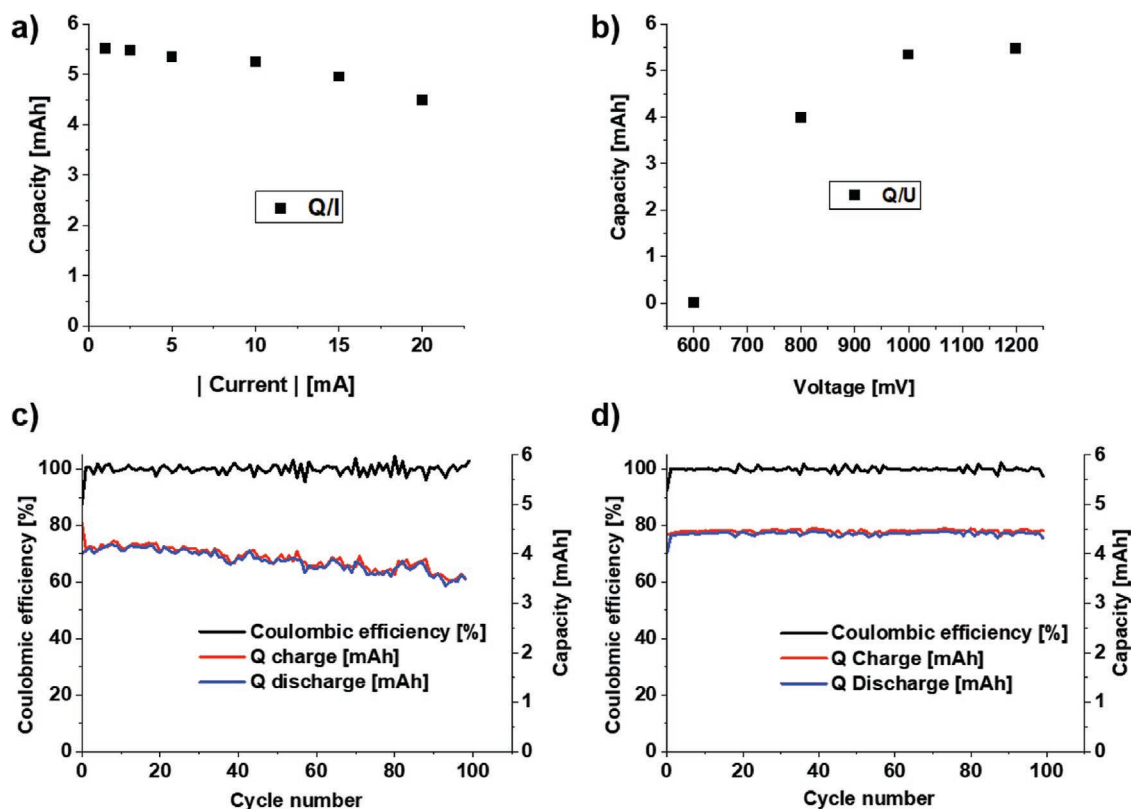
After battery equilibration, the cell was charged and the charged state was held for 24 h in order to check for possible side reactions or precipitation of the material. As such were absent, 100 charge-discharge cycles with 5 mA current were run at ambient temperature (Figure S21, Supporting Information) in order to evaluate potential capacity fade of the battery system. A stable coulombic efficiency of 99.88% was obtained. However, the battery revealed a significant capacity fade of ≈10% over the first 100 cycles or ≈0.02 mAh per day. This can be attributed to the occurrence of osmotic processes between the battery half-cells.[44] The initial capacity of the battery could be restored by adding water (5 mL) to the reservoir of the P2 containing solution. The observed

behavior and appropriate handling were already reported in another study.[27b] The current was varied in order to test the battery capacity at different charge and discharge currents (**Figure 3**a). The minimum charge current tested was 1 mA, which corresponds to 0.2 mA cm^{-2}. Increasing the charging current of the battery to 20 mA reduced the capacity by only 20%. Before applying a current of 2.5 mA, water (5 mL) was added one last time to enable sufficient convection of the electrolyte solution.

In additional experiments, the voltage was varied. As already indicated by the CV measurements, a charging voltage of 800 mV is necessary to charge the battery to 3.99 mAh and voltages of >1 V to yield an experimental[9e] capacity of 5.47 mAh, which is 70% of the theoretical maximum capacity, as determined from results of cerimetric titration (Figure 3b).

After measuring the current- and the voltage-dependent apparent capacity, the same battery was cycled for another 100 charge-discharge cycles at the same conditions as for the first 100 cycles with 5 mA current up to 1 V (Figure S22, Supporting Information). Over 100 cycles (10 d), the maximum apparent capacity decreased only as little as 0.1 mAh overall (≈2% of the maximum charge of 5.47 mAh or ≈0.01 mAh per day). Notably, the capacity curves revealed a strongly linear trend. However, a higher apparent discharge capacity over the apparent charge capacity could be observed. This was already the case for the last voltage-capacity dependence experiments.

The cycling was continued for 100 cycles at 20 mA (Figure 3c), a current well within the typical range of other applied polymeric active materials.[29] An overall capacity loss of ≈0.7 mAh (0.28 mAh per day) was observed. However, the Coulombic efficiency was still at 99.88%, remaining stable over more than 300 overall cycles. The capacity drop may be attributed to slower kinetics of the discharge process, as 0.7 mAh could be extracted from the cell when the discharge

ADVANCED
SCIENCE NEWS
www.advancedsciencenews.com

ADVANCED
ENERGY
MATERIALS
www.advenergymat.de

Figure 3. Battery characteristics of the polymer P1 versus BTMAPV 7 RFB. a) The apparent discharge capacity was measured at different charge and discharge currents within voltage limits of $V_{max} = 1$ V and $V_{min} = 0.4$ V. b) The apparent discharge capacity was measured at different upper voltage limits during charging with a fixed current of $I = 5$ mA. c) Cycling of the battery at ambient temperature with 4 mA cm^{-2} up to $V_{max} = 1$ V and $V_{min} = 0.4$ V. d) Cycling of the battery at 60 °C reservoir temperature with 4 mA cm^{-2} up to $V_{max} = 1$ V and $V_{min} = 0.4$ V.

voltage was held for an extended time (Figure S23, Supporting Information).

Next, the battery was cycled at elevated temperature (the reservoirs were kept at 60 °C), in order to explore the thermal stability of the battery system. The battery was cycled under conditions as in the above described experiments. The elevated temperature increased the overall apparent capacity of the battery approximately by an additional 10% (Figure 3d). Assignment of a capacity loss was difficult as the slope of the linear fit of the capacity over time was slightly larger than 1 with a poor R^2 value. The corresponding voltage and current versus time plots can be found in Figure S25, Supporting Information.

As mentioned above, we assumed a polymer-structure-viscosity related cause. Investigation of the viscosity (Figure S30, Supporting Information) revealed that the absolute viscosity is, as expected, strongly affected by the temperature, which, for pure water, decreased from $\eta_0 = 0.89$ mPas at 25 °C to $\eta_0 = 0.48$ mPas at a temperature of 60 °C. The relative viscosity ($\eta_r = \eta_c/\eta_0$) of the polymer solution was strongly influenced by the addition of salt to the measured solution, a clear indicator of the polyelectrolyte effect changing the conformation of the polymer in solution. This can be seen by a significant reduction of the relative viscosity by the addition of salt, while the contribution of the polymer to the viscosity of the solution was independent of the temperature. As diffusion processes are expected to be much more rapid in solvents of lower

viscosity, the better overall performance of the battery at 60 °C can be explained by the overall lower solution viscosity and the increase in diffusion coefficients. This effect is also apparent in cyclic voltammetry, as can be seen in Figure S19, Supporting Information, where the peak current significantly increased at 60 °C when compared to 25 °C and a decrease of the peak split of ≈15 mV could be observed.

Temperature-dependent investigations of vanadium RFBs revealed that the potential peak splits of the redox-active materials shift toward smaller peak potential gaps with increasing temperature, thus increasing the voltage efficiency.[45] Furthermore, higher temperatures increase the ion mobility in solutions, thus decreasing the ionic resistance. For example, when graphite is used as current collector, the ohmic resistance of the cell is also reduced with rising temperature.[46]

In our case, the cell performance improved when the active material was cycled at 60 °C, in contrast to the experiments at ambient temperature, proving the material being not only stable enough for drastic conditions in warm locations but also drawing benefits from the increased temperature.

The stability of the active material in the charged state at 60 °C was accessed by keeping the battery in an open circuit condition, while the electrolyte was continuously pumped with a flow rate of 30 mL min^{-1}, i.e., the same flow rate as for the other experiments, for 24 h after charging. The open circuit
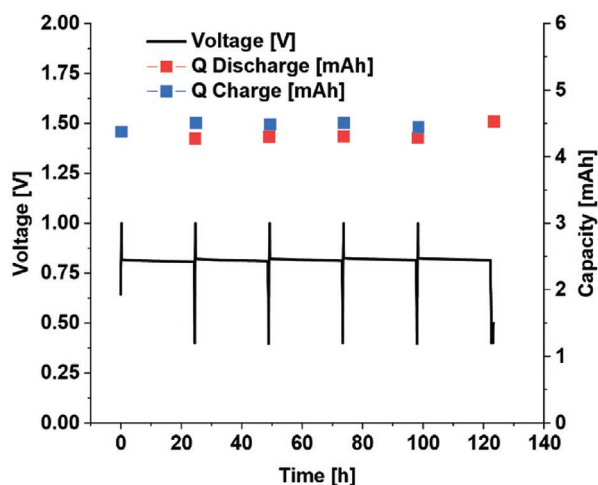
Figure 4. Stability experiment of the charged state and the voltage of the battery over the cycle number. The electrolyte reservoirs were kept at 60 °C and charged with 20 mA to 1 V. After reaching the limiting voltage, the electrolyte was continuously pumped for the OCV test where one cycle lasted 24 h. It was then discharged with 20 mA to 0.4 V. After the last cycle, the discharge voltage and current were held for 30 min to retrieve "trapped" charges in the polymer.

voltage as well as the apparent discharge capacity was monitored (**Figure 4**).

The system shows little self-discharge, thus again proving the suitability for energy storage under warm conditions.

2.4. Evaluation of the Thermal Stability of the Electrolytes

The temperature stability of the electrolytes was further investigated by ^{1}H NMR. For this purpose, the uncharged electrolytes with the same concentrations as in the battery were dissolved in D_2O and stored at 60 °C for two weeks. No changes in the ^{1}H NMR spectrum of BTMAPV 7 (Figure S31, Supporting Information) were visible, neither any optical changes like precipitation or a change in color appeared. This confirms the exceptional stability of the molecule in the uncharged state in pure water. In a next setup, the stability at 60 °C was also investigated in concentrated salt solutions (Figure S33, Supporting Information). After one night, the formation of cubic salt crystals could be observed but no clouding or color changes. Finally, BTMAPV 7 was charged in a static battery setup and stored at ambient temperature as well as at 60 °C for one week in an argon-filled glovebox (Figure S34, Supporting Information). After one week, no visible changes of the very dark blue solution could be observed.

Subsequently, ferrocene-containing polymer P2 was subjected to the very same tests. Small amounts of red precipitate were found after storing the uncharged polymer P2 in D_2O at 60 °C for two weeks (Figure S32, Supporting Information), possibly hinting towards the formation of iron oxides. Notably, the solution turned to dark green. Both changes may be caused by oxidation through oxygen. The salt-water solution of polymer P2, which was stored at 60 °C for two weeks (Figure S33, Supporting Information) showed darkening of the otherwise clear solution and formation of cubic crystals, which is most likely sodium chloride. However, the solution is void of any other precipitate. The charged polymer P2 was also stored at 60 °C (Figure S34, Supporting Information) and at ambient temperature in an argon-filled glovebox. After one week, the typical blue coloration from the charged ferrocene turned into dark green, indicating little self-discharge, while the solution at ambient temperature retained its coloration.

3. Conclusion

In this work, we presented the synthesis of a new ferrocene methacrylamide monomer in a four-step reaction with an overall yield of 50%. The ferrocene monomer was successfully copolymerized with a water-soluble comonomer via free-radical polymerization, which yielded four polymers with different comonomer ratios between 13% and 32% ferrocene content, as determined by cerimetric titration. The absolute molar mass of the polymer was investigated via SEC-MALLS. Electrochemical characterization revealed that the redox potential of the ferrocene polymer ($E_{1/2} = 0.52$ V) in an aqueous environment is slightly higher compared to the previously published low molar mass ferrocene derivatives. The diffusion coefficient for the polymer was determined by RDE and synthetic boundary experiments with an analytical ultracentrifuge. The obtained values from both techniques ($D_{app} = 9.8 \times 10^{-7}$ cm² s^{-1} from RDE and $D_{app} = 7.6 \times 10^{-7}$ cm² s^{-1} from synthetic boundary experiments for P2) are of the same order of magnitude, validating the applicability of both methods. Battery testing revealed stable cycling behavior for the polymer over 100 cycles of charging and discharging at ambient temperature and 60 °C with an average coulombic efficiency of over 99.8% through all cycling experiments. Investigations of the temperature stability revealed that the herein presented active materials not only easily withstand elevated temperatures, but that these conditions actually aid the electrochemical processes. This renders the need for expensive cooling solutions and careful consideration of the environmental impacts unnecessary. To the best of our knowledge, this is the first example of an aqueous, polymeric redox flow battery, that is able to deal with extreme conditions such as heat and strongly saline solutions, enabling the installation of more environmentally friendly, cheap energy storage solutions in temperature critical places, such as in near-equator countries.

Supporting Information

Supporting Information is available from the Wiley Online Library or from the author.

Acknowledgements

Conflict of Interest

The authors declare no conflict of interest.

Keywords

[1] a) D. O. Akinyele, R. K. Rayudu, *Sustainable Energy Technol.* **2014**, *8*, 74; b) H.-W. Sinn, *Eur. Econ. Rev.* **2017**, *99*, 130.

[2] P. Alotto, M. Guarnieri, F. Moro, *Renewable Sustainable Energy Rev.* **2014**, *29*, 325.

[3] Á. Cunha, J. Martins, N. Rodrigues, F. P. Brito, *Int. J. Energy Res.* **2015**, *39*, 889.

[4] J. A. J. Watt, I. T. Burke, R. A. Edwards, H. M. Malcolm, W. M. Mayes, J. P. Olszewska, G. Pan, M. C. Graham, K. V. Heal, N. L. Rose, S. D. Turner, B. M. Spears, *Environ. Sci. Technol.* **2018**, *52*, 11973.

[5] A. Bhattacharjee, H. Saha, *Appl. Energy* **2018**, *230*, 1182.

[6] K. Gong, X. Ma, K. M. Conforti, K. J. Kuttler, J. B. Grunewald, K. L. Yeager, M. Z. Bazant, S. Gu, S. Yan, *Energy Environ. Sci.* **2015**, *8*, 2941.

[7] C. A. Aubin, S. Choudhury, R. Jerch, L. A. Archer, J. H. Pikul, R. F. Shepherd, *Nature* **2019**, *571*, 51.

[8] K. L. Hawthorne, J. S. Wainright, R. F. Savinell, *J. Electrochem. Soc.* **2014**, *161*, A1662.

[9] a) J. Winsberg, T. Hagemann, T. Janoschka, M. D. Hager, U. S. Schubert, *Angew. Chem., Int. Ed.* **2017**, *56*, 686; *Angew. Chem.* **2017**, *129*, 702; b) R. Chen, D. Bresser, M. Saraf, P. Gerlach, A. Balducci, S. Kunz, D. Schröder, S. Passerini, J. Chen, *ChemSusChem* **2020**, *13*, 2205; c) V. Singh, S. Kim, J. Kang, H. R. Byon, *Nano Res.* **2019**, *12*, 1988; d) S. Jin, E. M. Fell, L. Vina-Lopez, Y. Jing, P. W. Michalak, R. G. Gordon, M. J. Aziz, *Adv. Energy Mater.* **2020**, *10*, 2000100; e) D. G. Kwabi, Y. Ji, M. J. Aziz, *Chem. Rev.* **2020**, *120*, 6467.

[10] Z. Huang, P. Zhang, X. Gao, D. Henkensmeier, S. Passerini, R. Chen, *ACS Appl. Energy Mater.* **2019**, *2*, 3773.

[11] R. R. Gagne, C. A. Koval, G. C. Lisensky, *Inorg. Chem.* **1980**, *19*, 2854.

[12] A. Mayyas, D. Steward, M. Mann, *Sustainable Mater. Technol.* **2019**, *19*, e00087.

[13] D. H. P. Kang, M. Chen, O. A. Ogunseitan, *Environ. Sci. Technol.* **2013**, *47*, 5495.

[14] D. Astruc, *Eur. J. Inorg. Chem.* **2017**, *2017*, 6.

[15] M. Patra, G. Gasser, *Nat. Rev. Chem.* **2017**, *1*, 0066.

[16] M. Saleem, H. Yu, L. Wang, A. Zain ul, H. Khalid, M. Akram, N. M. Abbasi, J. Huang, *Anal. Chim. Acta* **2015**, *876*, 9.

[17] C. Su, Y. Ye, L. Xu, C. Zhang, *J. Mater. Chem.* **2012**, *22*, 22658.

[18] Y. Zhao, Y. Ding, J. Song, G. Li, G. Dong, J. B. Goodenough, G. Yu, *Angew. Chem., Int. Ed.* **2014**, *53*, 11036; *Angew. Chem.* **2014**, *126*, 11216.

[19] a) Y. Ding, Y. Zhao, Y. Li, J. B. Goodenough, G. Yu, *Energy Environ. Sci.* **2017**, *10*, 491; b) M. Milton, Q. Cheng, Y. Yang, C. Nuckolls, R. Hernández Sánchez, T. J. Sisto, *Nano Lett.* **2017**, *17*, 7859; c) X. Wei, L. Cosimbescu, W. Xu, J. Z. Hu, M. Vijayakumar, J. Feng, M. Y. Hu, X. Deng, J. Xiao, J. Liu, V. Sprenkle, W. Wang, *Adv. Energy Mater.* **2015**, *5*, 1400678; d) B. Hwang, M.-S. Park, K. Kim, *ChemSusChem* **2015**, *8*, 310.

[20] a) E. S. Beh, D. De Porcellinis, R. L. Gracia, K. T. Xia, R. G. Gordon, M. J. Aziz, *ACS Energy Lett.* **2017**, *2*, 639; b) B. Hu, C. DeBruler, Z. Rhodes, T. L. Liu, *J. Am. Chem. Soc.* **2017**, *139*, 1207.

[21] G. Cong, Y. Zhou, Z. Li, Y.-C. Lu, *ACS Energy Lett.* **2017**, *2*, 869.

[22] W. Crawford, W. E. Watts, *J. Organomet. Chem.* **1976**, *110*, 257.

[23] G. Mwande Maguene, J.-B. Lekana-Douki, E. Mouray, T. Bousquet, P. Grellier, S. Pellegrini, F. S. Toure Ndouo, J. Lebibi, L. Pélinski, *Eur. J. Med. Chem.* **2015**, *90*, 519.

[24] K. Tappe, P. Knochel, *Tetrahedron: Asymmetry* **2004**, *15*, 91.

[25] J. K. Lindsay, C. R. Hauser, *J. Org. Chem.* **1957**, *22*, 355.

[26] V. Kovac, V. Rapic, J. Alagic, L. Barisic, *Croat. Chem. Acta* **1999**, *72*, 103.

[27] a) S. Muench, A. Wild, C. Friebe, B. Häupler, T. Janoschka, U. S. Schubert, *Chem. Rev.* **2016**, *116*, 9438; b) T. Hagemann, M. Strumpf, E. Schröter, C. Stolze, M. Grube, I. Nischang, M. D. Hager, U. S. Schubert, *Chem. Mater.* **2019**, *31*, 7987.

[28] a) J. Winsberg, T. Hagemann, S. Muench, C. Friebe, B. Häupler, T. Janoschka, S. Morgenstern, M. D. Hager, U. S. Schubert, *Chem. Mater.* **2016**, *28*, 3401; b) T. Janoschka, N. Martin, M. D. Hager, U. S. Schubert, *Angew. Chem., Int. Ed.* **2016**, *55*, 14427; *Angew. Chem.* **2016**, *128*, 14639; c) T. Janoschka, N. Martin, U. Martin, C. Friebe, S. Morgenstern, H. Hiller, M. D. Hager, U. S. Schubert, *Nature* **2015**, *527*, 78.

[29] Y. Y. Lai, X. Li, Y. Zhu, *ACS Appl. Polym. Mater.* **2020**, *2*, 113.

[30] E. C. Montoto, G. Nagarjuna, J. S. Moore, J. Rodríguez-López, *J. Electrochem. Soc.* **2017**, *164*, A1688.

[31] W. Yan, C. Wang, J. Tian, G. Zhu, L. Ma, Y. Wang, R. Chen, Y. Hu, L. Wang, T. Chen, J. Ma, Z. Jin, *Nat. Commun.* **2019**, *10*, 2513.

[32] F. S. Arimoto, A. C. Haven, *J. Am. Chem. Soc.* **1955**, *77*, 6295.

[33] X. Mao, F. Simeon, D. S. Achilleos, G. C. Rutledge, T. A. Hatton, *J. Mater. Chem. A* **2013**, *1*, 13120.

[34] a) J. Xiang, K. Sato, H. Tokue, K. Oyaizu, C.-L. Ho, H. Nishide, W.-Y. Wong, M. Wei, *Eur. J. Inorg. Chem.* **2016**, *2016*, 1030; b) S. M. Beladi-Mousavi, S. Sadaf, L. Walder, M. Gallei, C. Rüttiger, S. Eigler, C. E. Halbig, *Adv. Energy Mater.* **2016**, *6*, 1600108.

[35] T. Janoschka, S. Morgenstern, H. Hiller, C. Friebe, K. Wolkersdörfer, B. Häupler, M. D. Hager, U. S. Schubert, *Polym. Chem.* **2015**, *6*, 7801.

[36] C. U. Pittman, J. C. Lai, D. P. Vanderpool, M. Good, R. Prado, *Macromolecules* **1970**, *3*, 746.

[37] I. U. Khand, T. Lanez, P. L. Pauson, *J. Chem. Soc., Perkin Trans. 1* **1989**, *1*, 2075.

[38] G. D. Broadhead, J. M. Osgerby, P. L. Pauson, *J. Chem. Soc.* **1958**, 650.

[39] a) P. T. N. Nonjola, U. Siegert, J. C. Swarts, *J. Inorg. Organomet. Polym. Mater.* **2015**, *25*, 376; b) G. Chatelain, A. Meyer, F. Morvan, J.-J. Vasseur, C. Chaix, *New J. Chem.* **2011**, *35*, 893; c) Y. Yang, Z. Xie, C. Wu, *Macromolecules* **2002**, *35*, 3426.

[40] M. Grube, M. N. Leiske, U. S. Schubert, I. Nischang, *Macromolecules* **2018**, *51*, 1905.

[41] M. Grube, I. Perevyazko, T. Heinze, U. S. Schubert, I. Nischang, *Carbohydr. Polym.* **2020**, *229*, 115452.

[42] A. Neudeck, F. Marken, R. G. Compton, *Electroanalysis* **1999**, *11*, 1149.

[43] J. Winsberg, C. Stolze, A. Schwenke, S. Muench, M. D. Hager, U. S. Schubert, *ACS Energy Lett.* **2017**, *2*, 411.

[44] S. Yin, L. Zhou, X. Du, Y. Yang, *Ionics* **2019**, *25*, 593.

[45] T. Hagemann, J. Winsberg, M. Grube, I. Nischang, T. Janoschka, N. Martin, M. D. Hager, U. S. Schubert, *J. Power Sources* **2018**, *378*, 546.

[46] C. Zhang, T. S. Zhao, Q. Xu, L. An, G. Zhao, *Appl. Energy* **2015**, *155*, 349.